

Gravitational Wave Interference via Gravitational Lensing: Measurements of Luminosity Distance, Lens Mass, and Cosmological Parameters

Shaoqi Hou, Xi-Long Fan,^{*} and Kai Liao

School of Physics and Technology, Wuhan University, Wuhan, Hubei 430072, China

Zong-Hong Zhu[†]

School of Physics and Technology, Wuhan University, Wuhan, Hubei 430072, China and

Department of Astronomy, Beijing Normal University, Beijing 100875, China

(Dated: November 11, 2019)

The gravitational lensing of gravitational waves might cause beat patterns detectable by interferometers. The feature of this kind of signal is the existence of the beat pattern in the early inspiral phase, followed by seemingly randomly changing profile. After the strain peaks for the first time, the signal takes the usual waveform and the strain peaks for the second time. Once this signal is detected, the actual magnification factors can be obtained, so the true luminosity distance of the binary system is known. We can also infer the mass of the lens and the cosmological parameters with unprecedented precision due to the high accuracy in the measurement of the waveform.

I. INTRODUCTION

The existence of the gravitational wave (GW) has been confirmed by the 11 GW events observed by LIGO/Virgo collaborations [1]. Like the electromagnetic wave, GWs propagate at the speed of light c , and polarize in the direction perpendicular to their propagation directions [2]. Due to the equivalence principle, the trajectory of the GW bends when there is a gravitational potential near its way. This leads to the gravitational lensing effect [3, 4]. The lensing could cause the magnification in the GW amplitude, making it easier to be detected. However, this also leads to the underestimate of the luminosity distance of the GW source [5, 6].

GWs produced by the binary systems have much longer wavelengths than the (visible) light, so the wave optics effects [3, 7–10] would be strong if the lens is not massive enough. For GWs detectable by the ground-based detectors (1 - 10⁴ Hz), the geometric optics works if the mass of the lens is larger than about 10⁴ M_{\odot} , while for GWs with the frequencies in the LISA band (10⁻⁴ - 10⁻¹ Hz), the lens mass should be at least 10⁸ M_{\odot} [11, 12]. Despite some interesting phenomena (e.g., diffraction) due to the wave optics [8, 13], we would like to concentrate on the geometric optics. In this case, the lensed GWs travel in distinct paths, and arrive at the Earth at different times.

In this work, we will consider the strong lensing effect of the GW. More specifically, the time delay Δt between lensed GWs should be on the order of merely a few seconds if they are to be detected by the ground-based interferometers, while if the space-borne detectors are used, Δt can be as long as a few months. In this case, these detectors would observe the lensed GWs simultaneously. Since the binary system produces nearly monochromatic

GWs, and the GWs emitted in distinct directions carry definite phase differences from each other [14], a beat pattern appears in the time domain. Gradually, the beat pattern fades, since the frequency difference grows larger compared to their average. After the merger is observed along the earlier GW, the beat pattern quickly diminishes and the usual waveform emerges. As long as such kind of behavior is observed, one infers that the GWs were *probably* lensed [8]. This scenario allows us to infer the magnification factors of the amplitudes, then the absolute magnification factors can be determined, which determines the correct luminosity distance. One can also directly measure Δt very accurately from the observed waveform without the aid of the electromagnetic counterparts. With these information and assuming suitable lens models, the redshifted lens mass or the cosmological parameters can be determined.

In order to form the beat pattern, the constraint on Δt for the ground-based detectors is highly tight, so the probability of using the ground-based detectors to find beats is tiny. However, the requirement on Δt for the space-borne detectors is much relaxed, which implies that it is more plausible to use the detectors such as LISA to detect the beat pattern. In spite of the low probability associated with the ground-based detectors, we will start with the discussion on the beats detected by these detectors. This is because during the observation period, the motion of the Earth can be ignored, which makes the analysis simpler. The analysis of the beats observed by the space-borne detectors is more complicated as the detectors are moving in space during the observation, and their motion constantly changes the antenna pattern functions [15]. But if the beat period is in the range of a few hours to a few minutes, it is a good approximation to ignore the motion of the space-borne detectors. So once we understand how the ground-based detectors detect the beat pattern and make use of it, we can easily generalize that to the space-borne detectors.

Moreover, in the discussion on the beat pattern ob-

^{*} xilong.fan@whu.edu.cn

[†] zhuzh@whu.edu.cn

served by the ground-based detectors, we use the simple lens model of a point mass to illustrate the formation of the beats, the conditions and the applications. In contrast, for the space-borne detectors, the lens is chosen to be a singular isothermal sphere (SIS) [3]. The stars in galaxies may cause microlensing that also leads to the modulation in the GW amplitude. By Ref. [16], the effect of the microlensing is prominent when the magnification of the strong lensing is about a few hundreds to a few thousands, that is, when the saturation regime is reached. In the following scenarios to be discussed, the saturation is never reached, so the microlensing effect is negligible. Even if the magnification of the strong lensing is very large in some situations, the microlensing effect might also be less significant, because the beat pattern considered in our work exists in the (early) inspiral phase, and the microlensing induces modulation in higher frequency range (\sim a few hundred Hz) [16]. Therefore, in our discussion, we ignored the microlensing effect.

GW sources can be used as the standard sirens to measure their luminosity distances [17]. However, the gravitational lensing, in particular, the weak lensing makes the measurement less accurate with the uncertainty around a few percent [18]. This can be partially mitigated by utilizing the shear and flexion maps to infer the convergence and thus the magnification [19, 20]. The uncertainty in the luminosity distance can be reduced by 50%. The remaining uncertainty will inevitably affect our analysis, which should be considered in more realistic analysis. In this work, we neglect the effect of the weak lensing.

In Ref. [21], the interference between lensed GWs was also investigated within the geometric optics regime. The author did not use this interference to determine the luminosity distance, the lens mass or infer cosmological implications. Gravitational lensing has a wide range of applications, for example, detecting dark matter [22–25], constraining the speed of light [26], determining the cosmological constant [27–29], and examining the wave nature of GWs [13, 30]. Although no gravitational lensing signals have been detected in the observed GW events, the advent of more sensitive GW detectors might make it possible soon [31].

In the following, we start with a brief review on the gravitational lensing of GWs in Sec. II. Then we discuss the formation of the beat pattern observable by the ground-based interferometers in Sec. III. There, Sec. III A discusses generally the formation and the features of the beat pattern; Sec. III B is devoted to the signal-to-noise ratio (SNR) of such kind of signal; and finally, Sec. III C focus on the application of the beat pattern to determine the redshifted lens mass. In Sec. IV, we generalize the previous analysis to the space-borne detectors, in particular, LISA. In Sec. IV A, the formation and the SNR of the beat detected by LISA are presented, and in Sec. III C, the application of the beat pattern to constrain cosmological parameters is speculated. Of course, in both III and IV, how to determine the actual luminosity distance of the GW source is discussed. Finally, Sec. V summarizes

this work. In this work, the geometric units ($G = c = 1$) are used.

II. GRAVITATIONAL LENSING OF GRAVITATIONAL WAVES

In the geometric optics limit, GWs propagating in a generic, curved background interact with the background and experience three effects. First, the GW is described by gravitons, traveling in null geodesics. Second, the number of gravitons is conserved along the trajectory and the polarization plane rotates as the trajectory bends [14]. Since the deflection angle is very small, this rotation is ignored in this work. Third, the gravitational Faraday rotation occurs at the higher orders, so will also be ignored [32].

Figure 1 shows a typical geometry of a lens. The lens is labeled by L, and two GW rays (1 and 2) pass by it in two trajectories. The angles θ_{\pm} are between the lensed rays and the optical axis OL, with O labeling the observer. There are many different lens models. In the simplest case, the lens is a point mass M . Then one has [3]

$$\theta_{\pm} = \frac{1}{2}(\beta \pm \sqrt{\beta^2 + 4\theta_E^2}), \quad (1)$$

where β is the misalignment angle between the optical axis and the direction from the observer to the source of the GW, and $\theta_E = \sqrt{4M \frac{D_{LS}}{D_S D_L}}$ is the Einstein angle. $D_L = D(z_L)$ and $D_S = D(z_S)$ are the angular diameter distance $D(z)$ at redshifts z_L and z_S , respectively. D_{LS} is the angular diameter distance between the source and the lens. Since the probabilities for lensed GWs from the neutron star-neutron star mergers and the black hole-black hole mergers peak at redshifts about 2 and 4 [33], respectively, in this work, we are considering the sources at about $z = 2$ as examples. Due to the focusing effect of the lens, the amplitudes of the two rays get magnified by factors of

$$\mu_{\pm} = \frac{|\theta_{\pm}|}{\sqrt{|\theta_+^2 - \theta_-^2|}}, \quad (2)$$

respectively. Finally, there is a time delay between the two rays, given by

$$\Delta t = 4M(1 + z_L) \left(\frac{\theta_+^2 - \theta_-^2}{2\theta_E^2} + \ln \frac{\theta_+}{-\theta_-} \right). \quad (3)$$

A more realistic lens model is SIS, which is suitable for the early-type galaxies, and has a major contribution to the strong lensing probability [34, 35]. In this model,

$$\theta_{\pm} = \beta \pm \theta_E, \quad (4)$$

where the Einstein angle is $\theta_E = 4\pi\sigma_v^2 D_{LS}/D_S$ with σ_v the line-of-sight velocity dispersion of the stars in the

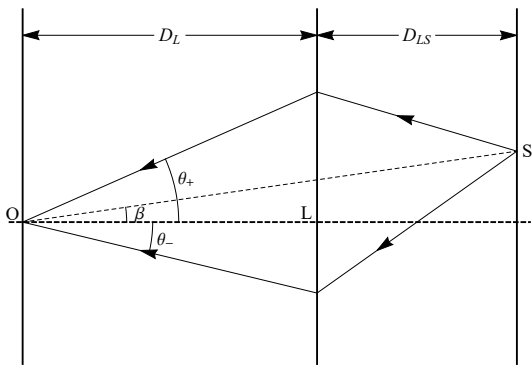


FIG. 1. Geometry of a Schwarzschild lens.

galaxy. The magnification factors are

$$\mu_{\pm} = \sqrt{\left| \frac{\theta_{\pm}/\theta_E}{|\theta_{\pm}/\theta_E| - 1} \right|}, \quad (5)$$

and the time delay is

$$\Delta t = 16\pi^2 \sigma_v^4 (1 + z_L) \frac{D_L D_{LS}}{D_S} \frac{\theta_+ + \theta_-}{\theta_E}. \quad (6)$$

In both models, the amplitudes of GWs get amplified by factors of μ_{\pm} after passing the lens. This would cause the underestimate of the luminosity distance of the source if the lensing effect is ignored. The time delays of many lensing systems are much longer than the observation periods of LIGO/Virgo, but usually shorter than that of LISA, depending on the mass function [36]. The particular scenario to be considered below provides the possibility to erase the effect of the lensing, and the true luminosity distance can be inferred, because the GW rays reach the detector simultaneously in certain time windows. Moreover, the luminosity distance, the lens mass and the cosmological parameters could also be obtained in the following scenario.

III. INTERFERENCE OBSERVED BY THE GROUND-BASED DETECTORS

A. Beat pattern

If there is a time window when the GW rays 1 and 2 reach the detector simultaneously, the strain is $h(t) =$

$h_1(t) + h_2(t)$, which can be schematically expressed as

$$\begin{aligned} h &= \mu_+ [A^+ \cos(\omega_1 t + \phi_1) + A^\times \sin(\omega_1 t + \phi_1)] \\ &\quad + \mu_- [A^+ \cos(\omega_2 t + \phi_2) + A^\times \sin(\omega_2 t + \phi_2)] \\ &= \mu_s [A^+ \cos(\omega_f t + \phi_f) \cos(\omega_b t + \phi_b) \\ &\quad + A^\times \cos(\omega_f t + \phi_f - \frac{\pi}{2}) \cos(\omega_b t + \phi_b)] + \\ &\quad \mu_d [A^+ \cos(\omega_f t + \phi_f + \frac{\pi}{2}) \cos(\omega_b t + \phi_b - \frac{\pi}{2}) \\ &\quad + A^\times \cos(\omega_f t + \phi_f) \cos(\omega_b t + \phi_b - \frac{\pi}{2})], \end{aligned} \quad (7)$$

where $A^{+/\times}$ stand for the amplitudes of the rays, $\mu_s = \mu_+ + \mu_-$ and $\mu_d = \mu_+ - \mu_-$. If these rays were generated by a binary system with masses m_1 and m_2 circling around each other, their amplitudes are roughly,

$$A^+ = \frac{4\mathcal{M}}{d_L} (\pi \mathcal{M} f)^{2/3} F^+ \frac{1 + \cos^2 \iota}{2}, \quad (8)$$

$$A^\times = \frac{4\mathcal{M}}{d_L} (\pi \mathcal{M} f)^{2/3} F^\times \cos \iota, \quad (9)$$

at the leading order, where $\mathcal{M} = (1 + z_S)(m_1 m_2)^{3/5}/(m_1 + m_2)^{1/5}$ is the redshifted chirp mass, d_L is the luminosity distance, ι is the inclination angle and $F^{+/\times}$ are the antenna pattern functions [15, 37]. In addition, ω_1 and ω_2 in Eq. (7) are the angular frequencies of the GWs, ϕ_1 and ϕ_2 are their initial phases, and

$$\omega_f = \frac{\omega_1 + \omega_2}{2}, \quad \phi_f = \frac{\phi_1 + \phi_2}{2}, \quad (10)$$

$$\omega_b = \frac{\omega_1 - \omega_2}{2}, \quad \phi_b = \frac{\phi_1 - \phi_2}{2}. \quad (11)$$

In the early inspiral phase, $2\omega_b$ is smaller than $2\omega_f$, because of the small time delay Δt , so beat pattern forms in the time domain with the beat frequency ω_b .

For the binary star system during the inspiral phase, the GW angular frequency evolves according to

$$\frac{d\omega}{dt} = \frac{192}{5} \mathcal{M}^{5/3} \left(\frac{\omega}{2}\right)^{11/3}, \quad (12)$$

at the leading order. When $\omega_b \ll \omega_f$, Eq. (12) can be used to calculate

$$\omega_b \approx \frac{96}{5} \left(\frac{\omega_f}{2}\right)^{11/3} \mathcal{M}^{5/3} \Delta t, \quad (13)$$

and ω_f is roughly the GW angular frequency. So as the time advances, ω_f increases and $\omega_b/\omega_f \propto \omega_f^{8/3}$ becomes larger. Eventually, the beat pattern disappears. After the compact-object merger is observed along ray 1, its strain drops dramatically, and the total strain is basically $h \approx h_2$, which has the same behavior as usual waveform with the amplitude magnified by a factor of μ_- .

With PyCBC [38], one can easily simulate the interference between the two GW rays 1 and 2. For example,

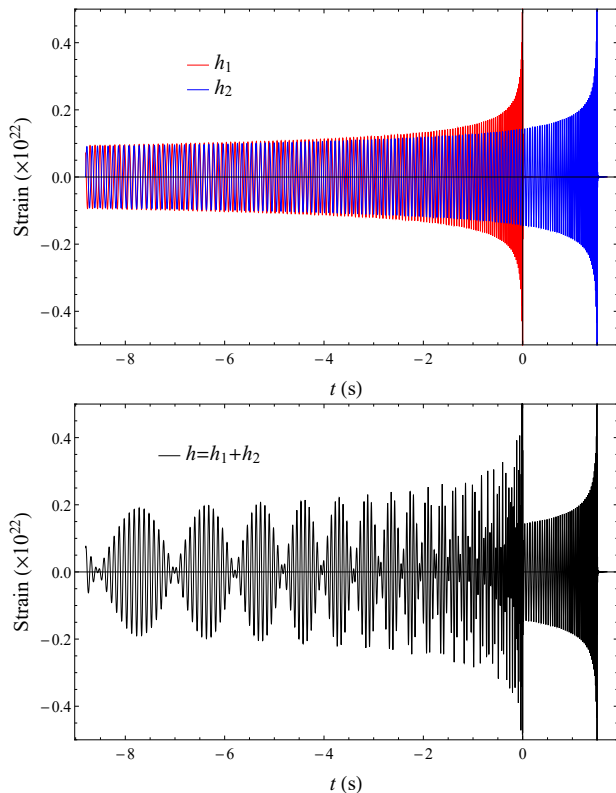


FIG. 2. The schematic diagrams showing the strains and the beat pattern in the time domain. In the two panels, the horizontal axes are time t in sec, and the vertical axes are strain $10^{22}h$.

let $m_1 = 30M_\odot$ and $m_2 = 20M_\odot$, and the binary system is assumed to be at $z_S = 2$. Suppose the lens is a point mass with $M = 10^6M_\odot$ and is at $z_L = 1$. Choose $\beta = 2.5 \times 10^{-5}$ arcsecond, then the magnification factors are $\mu_+ \approx 2.27$ and $\mu_- \approx 2.25$. With these choice of parameters, the time delay is $\Delta t \approx 1.49$ sec, which is small enough. Although β is very small, the wave optics can still be ignored because the time delay Δt is still much longer than the period of the GW in the detector bands [8]. For the purpose of demonstration, we assume that the two GR rays are parallel to each other as the deflection angles are $\alpha_1 \approx \alpha_2 \approx 3.6 \times 10^{-3}$ arcsecond. The inclination angle is chosen to be $\iota = 0$. Let the GWs travel in the direction perpendicular to the detector arms, then the strains h_1 , h_2 and h are shown in Fig. 2. The upper panel shows the strains h_1 and h_2 , separately. The lower panel shows the total strain $h = h_1 + h_2$. At the earlier time, e.g., $t \lesssim -2$ sec, there exists a fairly good beat pattern whose frequency ω_b increases with time. After -2 sec, the beat pattern gets disturbed due to the growth in ω_b/ω_f , and finally, it disappears. Although Fig. 2 is for the binary black hole merger, it is easy to understand that similar waveforms also apply to the binary neutron star and neutron star-black hole mergers.

The lower panel in Fig. 2 depicts the characteristic feature of the beat pattern. As long as one observes such

kind of events, one knows that the GWs were probably lensed [8]. Several quantities can be determined utilizing the lensed waveform. The beat frequency ω_b and the average frequency ω_f can be read off from the waveform in the early inspiral stage. The chirp mass \mathcal{M} is determined from the strain after the merger is observed through the first ray, and thus Eq. (13) gives Δt , which could also be read off from Fig. 2 by measuring the length from the first merge to the second. Therefore, the time delay can be determined without the aid of the electromagnetic counterpart in principle, with a *higher* precision on the order of ~ 0.1 sec.

B. Signal-to-noise ratio

The frequency domain waveform for the beat is also easy to be obtained, which is used to calculate the signal-to-noise ratio (SNR) [39]. Let $\tilde{h}_1(f)$ be the frequency domain waveform for $h_1(t)$, i.e.,

$$\tilde{h}_1(f) = \mu_+ \int_{-\infty}^{\infty} h_u(t) e^{i2\pi f t} dt, \quad (14)$$

where $h_u(t)$ is for the unlensed waveform, then the frequency domain waveform $\tilde{h}_2(f)$ for $h_2(t) = \frac{\mu_-}{\mu_+} h_1(t - \Delta t)$ is

$$\tilde{h}_2(f) = e^{i2\pi f \Delta t} \mu_- \tilde{h}_1(f). \quad (15)$$

So the total waveform is

$$\tilde{h}(f) = \sqrt{\mu_+^2 + \mu_-^2 + 2\mu_+\mu_- \cos(2\pi f \Delta t)} \tilde{h}_u(f), \quad (16)$$

where $\tilde{h}_u(f)$ represents the unlensed frequency domain waveform. Figure 3 shows the characteristic strains of the beat and the unlensed signals, together with the sensitivity curves of aLIGO, Einstein Telescope (ET) and Cosmic Explorer (CE) [40, 41]. It shows that the beat strain is highly oscillating in the frequency domain, due to the small Δt . In fact, the “period” of this oscillation is $1/\Delta t \approx 0.67$ Hz. The SNR’s for the signals presented

	aLIGO	ET	CE
beat	4.09	78.0	294
unlensed	1.28	24.3	91.8

TABLE I. SNR’s for the GW considered in Fig. 2. The detectors are chosen to be aLIGO, ET and CE. “unlensed” corresponds to the red or the blue signal in the upper panel of Fig. 2, and “beat” is for the signal in the lower panel.

in Fig. 2 can thus be calculated, assuming the detector is aLIGO, ET or CE, and tabulated in Table I. In this table, “unlensed” refers to the SNR calculated for the red or the blue signal in the upper panel of Fig. 2, while “beat” is for the beat signal in the lower panel. It is clear that the interference causes increases in SNR’s due to (1)

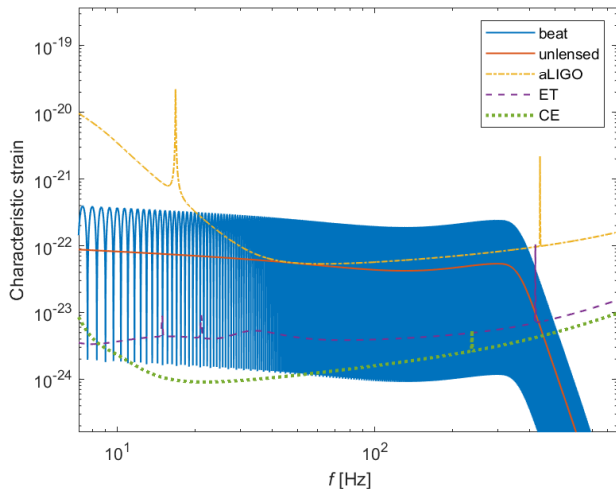


FIG. 3. The characteristic strains for the beat (solid blue curve) and the unlensed GW (solid brown curve) together with the sensitivity curves of aLIGO (dot-dashed yellow curve), ET (dashed purple curve) and CE (dotted green curve).

the amplification of the individual GW signal and (2) the simultaneous detection of them. One finds out that the beat has large enough SNR's if it is detected by ET or CE.

C. Application

Suppose such kind of signal can be detected with a high SNR, then one can make use of it to extract some useful information about the lens and even some cosmological parameters. By Eq. (7), it is possible to infer μ_s/μ_d by matched filtering once the template for the lensed GWs is used. If μ_d is too small to be determined, one can still obtain μ_s/μ_- by measuring the amplitude of h_2 using the data after the merger is detected through the first ray. So the relative magnification μ_+/μ_- is known,

$$\frac{\mu_+}{\mu_-} = \frac{1 + \mu_s/\mu_d}{1 - \mu_s/\mu_d} = \frac{\mu_s}{\mu_-} - 1, \quad (17)$$

which can be used to find the ratio $r_{\pm} = \theta_+/\theta_- = \mu_+/\mu_-$ with Eq. (2). Substituting r_{\pm} back into Eq. (2) gives the actual magnifications,

$$\mu_+ = \frac{1}{\sqrt{|1 - r_{\pm}^{-2}|}}, \quad \mu_- = \frac{1}{\sqrt{|r_{\pm}^2 - 1|}}. \quad (18)$$

With these, one can unambiguously calculate the luminosity distance of the source. Further, using r_{\pm} , Eqs. (1), and (2), one finds β/θ_E , which can be substituted into Eq. (3), with the help of Eq. (1), to find the redshifted lens mass,

$$M(1 + z_L) = \frac{\Delta t}{4} \left[\frac{1}{2} \left| r_{\pm} - \frac{1}{r_{\pm}} \right| + \ln(-r_{\pm}) \right]^{-1}. \quad (19)$$

The above application relies on the observation of several beats, so the observation time should be a few seconds, which can be achieved for the third generation detectors such as ET and CE. One can estimate how long an inspiral signal lasts given an initial frequency by integrating Eq. (12) to get the GW frequency,

$$f(t) = \left[f_c^{-8/3} - \frac{256\pi}{5} (\pi M)^{5/3} (t - t_c) \right]^{-3/8}, \quad (20)$$

and then, solving for $t - t_c$. Here, t_c is the fiducial coalescence time and f_c is the corresponding coalescence frequency. One may choose $f_c = f_{\text{iseco}}$ with [42]

$$f_{\text{iseco}} = 8.80(1 + 1.25\eta + 1.08\eta^2) \left[\frac{M_{\odot}}{(1 + z_S)(m_1 + m_2)} \right] \text{kHz}, \quad (21)$$

where $\eta = m_1 m_2 / (m_1 + m_2)^2$ is the symmetric mass ratio. This is the GW frequency when the inner-most stable circular orbit (ISCO) of the binary system is reached. Take the unlensed GW signal in the previous subsections for example. From Fig. 3, the unlensed signal is well above the sensitivity curves of ET and CE from 5 Hz, then using the above equation, one finds out that the time left to reach f_{iseco} is about 8.6 sec, which is long enough to contain several beat periods.

This application also calls for high enough lensing event rates. Several works discussed the lensing rates for LIGO [5] and ET [33, 43, 44]. At the design sensitivity, aLIGO could only detect about 5 lensed GW events per year, while the event rate increases to about 80 to 100 per year for ET. In their calculations, some more realistic lens models such as SIS were considered, and the lensed GW events were required to have high enough SNR's (≥ 8). The event rate for the beat pattern would be even smaller, because of the extreme restriction on Δt , or β . Although the rate will be calculated in the future work, here we roughly estimate it. Assuming the SIS model (in order to be more realistic), β should be around 10^{-7} arcsecond if the source and the lens are still at $z_S = 2$ and $z_L = 1$, respectively, and $\sigma = 250$ km/s [26]. The Einstein angle is $\theta_E = 0.65$ arcsecond, so $\beta/\theta_E \approx 10^{-6} \sim 10^{-7}$. Then by [45], the lensing cross section and thus the optical depth would be about 12 to 14 orders of magnitude smaller than those considered in Refs. [5, 33, 43, 44], so the lensing rate for the beat is much less than the predicted values quoted above.

For the space-borne interferometers, the restriction on β is much relaxed, and the lensing rate is expected higher. So in the next section, we will discuss the beat detectable by these detectors.

IV. INTERFERENCE OBSERVED BY THE SPACE-BORNE DETECTORS

From the above discussion, one finds out that in order to detect the beat pattern on the ground, there is

a tremendously tight bound on $\beta \sim 10^{-5} - 10^{-7}$ arcsecond. This leads to the extremely low probabilities to observe the beat pattern even with ET or CE. The tight bound is due to the small observation periods available to these detectors. In contrast, the target GWs of the spaceborne interferometers could last for much longer times. The formation of the beat pattern by lensing these GWs places milder constraint on β . It is useful to study the beat pattern observed by detectors such as LISA and the application.

The following discussion will parallel to that in the previous section III. In order to avoid the repetition, we will emphasize some of the differences, which are mainly the less restricted misalignment angle β , the longer and more beat periods.

A. Beat and its SNR

Before demonstrating a concrete example of a beat pattern, we should notice that LISA, for instance, is sensitive in frequency range $10^{-4} - 10^{-1}$ Hz. So one should expect that the beat period can be very long, as the beat angular frequency $\omega_b \ll \omega_f$ with ω_f roughly the GW angular frequency. If the beat period is too long, e.g., on the order of a few months, then the orbital motion of the LISA satellites would have some imprints on the interference pattern detected by LISA. This is due to the fact that the antenna pattern functions $F^{+/\times}$ [refer to Eqs. (8) and (9)] depend on the relative orientation of the GW to the constellation plane of LISA. So for a fixed GW source, LISA would register different strains at different positions in its orbit [15], as nicely demonstrated in Ref. [46]. This effect would make the analysis of the beat pattern more complicated, since $F^{+/\times}$ are effectively also functions of time t . However, ω_b grows over time by Eq. (13). Thus there is the possibility that ω_b becomes large enough such that the beat period is on the order of a few hours to a few minutes. When this happens, the orbital motion of LISA might be ignored. Although the varying $F^{+/\times}$ during the long beat periods do not fundamentally change the analysis of the beat, in the current work, we focus on the simpler case where the beat periods are small enough to ignore the orbital motion of LISA.

In order to make sure that there exists some time window when the beat periods are small enough to ignore the orbital motion of LISA, the time delay Δt should be big enough. But at the same time, Δt should also be bounded from above, otherwise ω_b would quickly increase to such a good portion of ω_f in a relatively short time that there are not enough beats for us to use. In the following, we will exhibit a binary system and a SIS lens to satisfy these conditions.

The suitable sources of GWs detectable by the spaceborne interferometers usually have much heavier masses than the above example. For example, one may consider a binary star system of masses $5 \times 10^4 M_\odot$ and $4 \times 10^4 M_\odot$ at the redshift $z_S = 2$. Let the lens be an early-type

galaxy with the velocity dispersion $\sigma = 250$ km/s [26]. Then set $\beta = 0.1$ arcsecond, resulting in $\theta_E = 0.65$ arcsecond, $\mu_+ \approx 2.75$, and $\mu_- \approx 2.35$. The time delay is $\Delta t = 1.05$ months, which is an appropriate value. Here, we display the frequency domain waveforms for the beat and the unlensed GW in Fig. 4, together with the sensitivity curve of LISA, using LISA sensitivity calculator [47, 48]. In this plot, the unlensed GW is represented

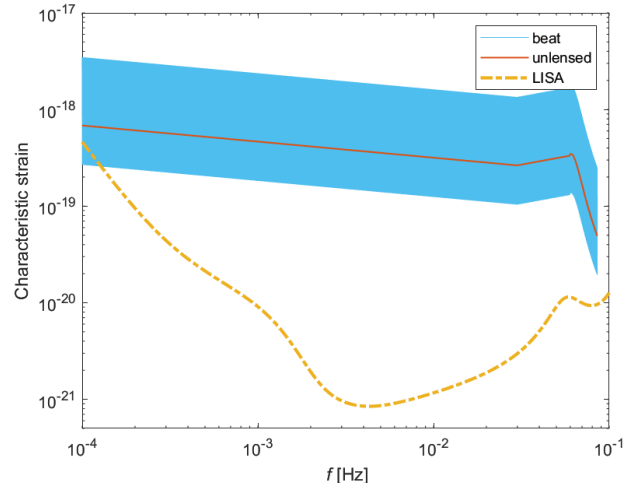


FIG. 4. The characteristic strains for the beat (solid cyan curve), the unlensed GW (solid brown curve) and the sensitivity curve of LISA (dot-dashed orange curve). This plot is generated using LISA sensitivity calculator [48].

by the solid brown curve, which is well above the sensitivity curve of LISA, the dot-dashed orange curve. One can easily calculate its SNR, which is approximately 517. The cyan curve is for the beat. According to Eq. (16), the strain of the beat $\tilde{h}(f)$ is oscillating in the frequency domain with the “period” $1/\Delta t \approx 3.66 \times 10^{-7}$ Hz. Such a small period makes the cyan curve curl up to form a band. Its SNR is about 1870.

Suppose this interfered signal can be detected from 10^{-4} Hz, then it can be estimated that f_{isco} is reached after nearly 1.36 years. Integrating Eq. (20) over time gives the phase of the GW,

$$\phi(t) = \phi_c + \frac{1}{16} \left\{ \frac{1}{(\pi \mathcal{M} f_c)^{5/3}} - \left[\frac{1}{(\pi \mathcal{M} f_c)^{8/3}} - \frac{256 t - t_c}{5 \mathcal{M}} \right]^{5/8} \right\}, \quad (22)$$

where ϕ_c is a fiducial coalescence phase. This facilitates the determination of the beat period more accurately. In fact, the phase for the beat is $\phi_b(t) = \phi(t) - \phi(t - \Delta t)$. Now, set $\cos \phi_b(t) = 0$, then one can solve this equation to determine the time t_n when $\phi_b(t_n) = (n + 1/2)\pi$ with n some integer, and $t_{n+1} - t_n$ is half of the beat period. It turns out that the periods for the first few beats are from about two weeks down to one or two days. So none of these beats can be used to easily extract

useful information. There are actually some beats with small enough periods, on the order of a few hours. These beats start from the time when there are just 10.6 months before the GW frequency reaches f_{ISCO} . In total, there are 407 such kind of beats, so it is possible to use them to extract some useful information as done in Sec. III C. The SNR for these beats is estimated to be 31.0.

B. Application

With the relations presented in the previous sections, one concludes that it is still possible to obtain the magnification factors. First, by Eq. (4), $\frac{\theta_+}{\theta_E} - \frac{\theta_-}{\theta_E} = 2$. Once the ratio $\alpha = \mu_+/\mu_-$ is inferred using the matched filtering as given by Eq. (17), these give,

$$\frac{\theta_+}{\theta_E} = \frac{\zeta(\alpha) + 1 + 3\alpha^2}{2(1 + \alpha^2)}, \quad \frac{\theta_-}{\theta_E} = \frac{\zeta(\alpha) - 3 - \alpha^2}{2(1 + \alpha^2)}, \quad (23)$$

where $\zeta(\alpha) = \sqrt{\alpha^4 + 14\alpha^2 + 17}$. These can be substituted back into Eq. (5) to calculate μ_{\pm} ,

$$\mu_+ = \sqrt{\frac{3 + 5\alpha^2 + \zeta(\alpha)}{1 + 3\alpha^2 + \zeta(\alpha)}}, \quad (24)$$

$$\mu_- = \sqrt{\frac{5 + 4\alpha^2 - \zeta(\alpha)}{-3 - \alpha^2 + \zeta(\alpha)}}. \quad (25)$$

Therefore, the actual luminosity distance of the source is also determined.

As discussed above, the time delay Δt can be measured by two different methods. One is to simply find the times of the two mergers and take their difference, and the other is to measure the beat frequency ω_b , which is substituted into Eq. (13) to solve for Δt . The second method is better in the sense that some GW signals merge at the higher frequencies beyond LISA's sensitive band. Now, since the early-type galaxy serves as the lens in the SIS model, it is possible to obtain the *galaxy's* redshift z_L using the natural electromagnetic signal [49]. Once z_L is known, Eq. (6) gives the time-delay distance $D_{\Delta t} = D_L D_{LS}/D_S$,

$$D_{\Delta t} = \frac{\Delta t}{16\pi^2 \sigma_v^2 (1 + z_L)} \frac{1 + \alpha^2}{\zeta(\alpha) - 1 + \alpha^2}. \quad (26)$$

In the Friedmann-Robertson-Walker spacetime, the angular diameter distance is given by [50],

$$D(z) = \frac{1}{\sqrt{\Omega_k} H_0 (1+z)} \times \sinh \left[\sqrt{\Omega_k} \int_{\frac{1}{1+z}}^1 \frac{dx}{\sqrt{\Omega_r + \Omega_m x + \Omega_k x^2 + \Omega_\Lambda x^4}} \right], \quad (27)$$

where H_0 is the present-day Hubble constant, and Ω_l are the density parameters for the radiation ($l = r$), the matter ($l = m$), the spatial curvature $l = k$ and the dark energy $l = \Lambda$, respectively. Therefore, $D_{\Delta t}$ could be used to constrain the cosmological parameters, especially the Hubble constant H_0 [29, 51]. For this purpose, one has to use the electromagnetic follow-up observations to determine the host galaxy of the GW source and thus z_S [18]. The advantage of using the beat pattern is that one needs not find all the ‘‘images’’ in order to determine the Fermat potential. So this method would be more accurate.

The conservative estimation of the lensing rate for LISA has been done in Ref. [27]. During a 5-year mission, there can be 4 multiple events detectable with $\text{SNR} \geq 8$. From the previous subsection, one finds out that in order to detect the beat pattern using LISA, β can be on the order of 0.1 arcsecond, which is not very restricted. In this case, $\beta/\theta_E \approx 0.15$, which, compared with y_{max} in Fig. 1 in Ref. [27], does not have the difference on a few orders of magnitude. So it is possible to observe the beat with LISA. More exact calculation of the event rate will be done in the future work.

V. CONCLUSION

As discussed above, when the time delay between the lensed GWs is small enough, it is possible to obtain the actual luminosity distance by making the good use of the beat pattern. The time delay Δt can be easily measured at a very high precision without the need for the electromagnetic counterpart. The gravitational lensing caused by a massive black hole also enables the measurement of the redshifted mass of the lens, which does not rely on any statistics method, but the event rate is negligible. Since space-borne interferometers have much longer observation periods, there would be more GW events with the beat pattern detected and the method presented above could put very stringent constraints on the cosmological parameters.

ACKNOWLEDGMENTS

We would like to thank Hai Yu for the constructive discussions. This work was supported by the National Natural Science Foundation of China under Grants Nos. 11633001 and the Strategic Priority Research Program of the Chinese Academy of Sciences, Grant No. XDB23000000.

[1] B. P. Abbott *et al.* (Virgo, LIGO Scientific), *Phys. Rev. Lett.* **116**, 061102 (2016), arXiv:1602.03837 [gr-qc];

Phys. Rev. Lett. **116**, 241103 (2016), arXiv:1606.04855

- [gr-qc]; Phys. Rev. Lett. **118**, 221101 (2017), arXiv:1706.01812 [gr-qc]; Phys. Rev. Lett. **119**, 141101 (2017), arXiv:1709.09660 [gr-qc]; Phys. Rev. Lett. **119**, 161101 (2017), arXiv:1710.05832 [gr-qc]; Astrophys. J. **851**, L35 (2017), arXiv:1711.05578 [astro-ph.HE]; B. P. Abbott *et al.* (LIGO Scientific, Virgo), Phys. Rev. X **9**, 031040 (2019), arXiv:1811.12907 [astro-ph.HE].
- [2] C. W. Misner, K. S. Thorne, and J. A. Wheeler, *Gravitation* (W. H. Freeman, San Francisco, 1973).
- [3] P. Schneider, J. Ehlers, and E. E. Falco, *Gravitational Lenses* (Springer, Berlin, Heidelberg, 1992) p. 560.
- [4] J. K. Lawrence, *Il Nuovo Cimento B* (1971-1996) **6**, 225 (1971); Phys. Rev. D **3**, 3239 (1971).
- [5] K. K. Y. Ng, K. W. K. Wong, T. Broadhurst, and T. G. F. Li, Phys. Rev. D **97**, 023012 (2018), arXiv:1703.06319 [astro-ph.CO].
- [6] L. Dai, T. Venumadhav, and K. Sigurdson, Phys. Rev. D **95**, 044011 (2017), arXiv:1605.09398 [astro-ph.CO].
- [7] T. T. Nakamura, Phys. Rev. Lett. **80**, 1138 (1998).
- [8] T. T. Nakamura and S. Deguchi, *Progress of Theoretical Physics Supplement* **133**, 137 (1999).
- [9] R. Takahashi and T. Nakamura, *Astrophys. J.* **595**, 1039 (2003), arXiv:astro-ph/0305055 [astro-ph].
- [10] R. Takahashi, *Astrophys. J.* **835**, 103 (2017), arXiv:1606.00458 [astro-ph.CO].
- [11] M. Arnaud-Varvella, M. C. Angonin, and P. Tourrenc, *Gen. Rel. Grav.* **36**, 983 (2004), arXiv:gr-qc/0312028 [gr-qc].
- [12] A. K. Meena and J. S. Bagla, (2019), arXiv:1903.11809 [astro-ph.CO].
- [13] K. Liao, M. Biesiada, and X.-L. Fan, *Astrophys. J.* **875**, 139 (2019), arXiv:1903.06612 [gr-qc].
- [14] S. Hou, X.-L. Fan, and Z.-H. Zhu, Phys. Rev. D **100**, 064028 (2019), arXiv:1907.07486 [gr-qc].
- [15] R. Schilling, *1st International LISA Symposium on Gravitational Waves Oxfordshire, England, July 9-12, 1996*, *Class. Quant. Grav.* **14**, 1513 (1997); G. Giampieri, *Mon. Not. Roy. Astron. Soc.* **289**, 185 (1997), arXiv:gr-qc/9704069 [gr-qc]; D. Liang, Y. Gong, A. J. Weinstein, C. Zhang, and C. Zhang, Phys. Rev. D **99**, 104027 (2019), arXiv:1901.09624 [gr-qc].
- [16] J. M. Diego, O. A. Hannuksela, P. L. Kelly, T. Broadhurst, K. Kim, T. G. F. Li, G. F. Smoot, and G. Pagano, *Astron. Astrophys.* **627**, A130 (2019), arXiv:1903.04513 [astro-ph.CO].
- [17] B. F. Schutz, *Nature* **323**, 310 (1986).
- [18] D. E. Holz and S. A. Hughes, *Astrophys. J.* **629**, 15 (2005), arXiv:astro-ph/0504616 [astro-ph].
- [19] C. Shapiro, D. Bacon, M. Hendry, and B. Hoyle, *Mon. Not. Roy. Astron. Soc.* **404**, 858 (2010), arXiv:0907.3635 [astro-ph.CO].
- [20] S. Hilbert, J. R. Gair, and L. J. King, *Mon. Not. Roy. Astron. Soc.* **412**, 1023 (2011), arXiv:1007.2468 [astro-ph.CO].
- [21] K. Yamamoto, Phys. Rev. D **71**, 101301(R) (2005), arXiv:astro-ph/0505116 [astro-ph].
- [22] C. Cutler and D. E. Holz, Phys. Rev. D **80**, 104009 (2009), arXiv:0906.3752 [astro-ph.CO].
- [23] S. Camera and A. Nishizawa, Phys. Rev. Lett. **110**, 151103 (2013), arXiv:1303.5446 [astro-ph.CO].
- [24] G. Congedo and A. Taylor, Phys. Rev. D **99**, 083526 (2019), arXiv:1812.02730 [astro-ph.CO].
- [25] S. Jung and C. S. Shin, Phys. Rev. Lett. **122**, 041103 (2019), arXiv:1712.01396 [astro-ph.CO].
- [26] X.-L. Fan, K. Liao, M. Biesiada, A. Piorkowska-Kurpas, and Z.-H. Zhu, Phys. Rev. Lett. **118**, 091102 (2017), arXiv:1612.04095 [gr-qc].
- [27] M. Sereno, A. Sesana, A. Bleuler, P. Jetzer, M. Volonteri, and M. C. Begelman, Phys. Rev. Lett. **105**, 251101 (2010), arXiv:1011.5238 [astro-ph.CO].
- [28] M. Sereno, P. Jetzer, A. Sesana, and M. Volonteri, *Mon. Not. Roy. Astron. Soc.* **415**, 2773 (2011), arXiv:1104.1977 [astro-ph.CO].
- [29] K. Liao, X.-L. Fan, X.-H. Ding, M. Biesiada, and Z.-H. Zhu, *Nature Commun.* **8**, 1148 (2017), [Erratum: *Nature Commun.*8,no.1,2136(2017)], arXiv:1703.04151 [astro-ph.CO].
- [30] L. Dai, S.-S. Li, B. Zackay, S. Mao, and Y. Lu, Phys. Rev. D **98**, 104029 (2018), arXiv:1810.00003 [gr-qc].
- [31] O. A. Hannuksela, K. Haris, K. K. Y. Ng, S. Kumar, A. K. Mehta, D. Keitel, T. G. F. Li, and P. Ajith, *Astrophys. J.* **874**, L2 (2019), arXiv:1901.02674 [gr-qc].
- [32] T. Piran and P. N. Saifer, *Nature* **318**, 271 (1985); T. Piran, P. N. Saifer, and R. F. Stark, Phys. Rev. D **32**, 3101 (1985); A. Wang, Phys. Rev. D **44**, 1120 (1991).
- [33] L. Yang, X. Ding, M. Biesiada, K. Liao, and Z.-H. Zhu, *Astrophys. J.* **874**, 139 (2019), arXiv:1903.11079 [astro-ph.GA].
- [34] E. L. Turner, J. P. Ostriker, and J. R. Gott, III, *Astrophys. J.* **284**, 1 (1984).
- [35] O. Moeller, M. Kitzbichler, and P. Natarajan, *Mon. Not. Roy. Astron. Soc.* **379**, 1195 (2007), arXiv:astro-ph/0607032 [astro-ph].
- [36] M. Oguri, *Mon. Not. Roy. Astron. Soc.* **480**, 3842 (2018), arXiv:1807.02584 [astro-ph.CO].
- [37] M. Isi and A. J. Weinstein, (2017), arXiv:1710.03794 [gr-qc].
- [38] T. Dal Canton *et al.*, Phys. Rev. D **90**, 082004 (2014), arXiv:1405.6731 [gr-qc]; S. A. Usman *et al.*, *Class. Quant. Grav.* **33**, 215004 (2016), arXiv:1508.02357 [gr-qc]; A. Nitz *et al.*, “gwastro/pycbc: Pycbc release v1.13.6,” (2019).
- [39] N. Yunes and X. Siemens, *Living Rev. Rel.* **16**, 9 (2013), arXiv:1304.3473 [gr-qc].
- [40] M. Punturo *et al.*, *Gravitational waves. Proceedings, 8th Edoardo Amaldi Conference, Amaldi 8, New York, USA, June 22-26, 2009*, *Class. Quant. Grav.* **27**, 084007 (2010).
- [41] B. P. Abbott *et al.* (LIGO Scientific), *Class. Quant. Grav.* **34**, 044001 (2017), arXiv:1607.08697 [astro-ph.IM].
- [42] C. Bonvin, C. Caprini, R. Sturani, and N. Tamanini, Phys. Rev. D **95**, 044029 (2017), arXiv:1609.08093 [astro-ph.CO].
- [43] X. Ding, M. Biesiada, and Z.-H. Zhu, *JCAP* **1512**, 006 (2015), arXiv:1508.05000 [astro-ph.HE].
- [44] S.-S. Li, S. Mao, Y. Zhao, and Y. Lu, *Mon. Not. Roy. Astron. Soc.* **476**, 2220 (2018), arXiv:1802.05089 [astro-ph.CO].
- [45] A. Piorkowska, M. Biesiada, and Z.-H. Zhu, *JCAP* **1310**, 022 (2013), arXiv:1309.5731 [astro-ph.CO].
- [46] Y. Gong, “The supplementary material for antenna transfer function (arXiv: 1901.09624),” (2019).
- [47] T. Robson, N. J. Cornish, and C. Liug, *Class. Quant. Grav.* **36**, 105011 (2019), arXiv:1803.01944 [astro-ph.HE].
- [48] N. Cornish, “eXtremeGravityInstitute/LISA Sensitivity: Version 1,” (2019).
- [49] Note this electromagnetic signal is not from the galaxy that contains the GW source.

- [50] S. Weinberg, *Cosmology* (Oxford, UK: Oxford Univ. Pr. (2008) 593 p, 2008).
- [51] B. Liu, Z. Li, and Z.-H. Zhu, *Mon. Not. Roy. Astron. Soc.* **487**, 1980 (2019), arXiv:1904.11751 [astro-ph.CO].